Comparison of Tropospheric Emission Spectrometer nadir water vapor retrievals with in situ measurements

Mark W. Shephard,[1] Robert L. Herman,[2] Brendan M. Fisher,[2] Karen E. Cady-Pereira,[1] Shepard A. Clough,[1] Vivienne H. Payne,[1] David N. Whiteman,[3] Joseph P. Comer,[3] Holger Vömel,[4] Larry M. Miloshevich,[5] Ricardo Forno,[6] Mariana Adam,[7] Gregory B. Osterman,[2] Annmarie Eldering,[2] John R. Worden,[2] Linda R. Brown,[2] Helen M. Worden,[2] Susan S. Kulawik,[2] David M. Rider,[2] Aaron Goldman,[8] Reinhard Beer,[2] Kevin W. Bowman,[2] Clive D. Rodgers,[9] Mingzhao Luo,[2] Curtis P. Rinsland,[10] Michael Lampel,[11] and Michael R. Gunson[2]

[1] Comparisons of Tropospheric Emission Spectrometer (TES) water vapor retrievals with in situ measurements are presented. Global comparisons of TES water vapor retrievals with nighttime National Centers for Environmental Prediction RS90/RS92 radiosondes show a small (<5%) moist bias in TES retrievals in the lower troposphere (standard deviation of ~20%), increasing to a maximum of ~15% bias (with standard deviation reaching ~40%) in the upper troposphere. This moist bias with respect to the sonde bias increases to a maximum of ~15% in the upper troposphere between ~300–200 hPa. The standard deviation in this region reaches values of ~40%. It is important to note that the TES reported water vapor comparison statistics are not weighted by the water vapor layer amounts. Global TES/radiosonde results are comparable with the Atmospheric Infrared Sounder reported unweighted mean of 25% and root-mean-square of ~55%. While such global comparisons help to identify general issues, inherent sampling errors and radiosonde measurement accuracy can limit the degree to which the radiosonde profiles alone can be used to validate satellite retrievals. In order to characterize the agreement of TES with in situ measurements in detail, radiance closure studies were performed using data from the Water Vapor Validation Experiment – Satellites/Sondes campaign from July 2006. Results indicate that estimated systematic errors from the forward model, TES measurements, in situ observations, retrieved temperature profiles, and clouds are likely not large enough to account for radiance differences between TES observations and forward model calculations using in situ profiles as input. Therefore, accurate validation of TES water vapor retrievals requires further campaigns with a larger variety of water vapor measurements that better characterize the atmospheric state within the TES field of view.

1. Introduction

[2] From a number of perspectives, water is the most important molecule in the earth's atmosphere. Knowledge of its vertical, horizontal and temporal distribution is critical for the understanding of a broad range of topics including convective, chemical, radiative and phase change processes. The fact that water exists in the atmosphere in all three phases (water vapor, liquid water, and ice cloud) is a key aspect of its importance. Water vapor and clouds provide the dominant modulation of atmospheric cooling rates, radiation to the surface and radiation to space [*Clough et al.*, 1992]. The distribution of water vapor is key to atmospheric chemistry, to numerical weather prediction, and to studies of climate change [*Raval and Ramanathan*, 1989]. The main objective for obtaining satellite retrieved water vapor measurements

---
[1]Atmospheric and Environmental Research Incorporated, Lexington, Massachusetts, USA.
[2]Jet Propulsion Laboratory, Pasadena, California, USA.
[3]Goddard Space Flight Center, NASA, Greenbelt, Maryland, USA.
[4]National Oceanographic and Atmospheric Administration, Boulder, Colorado, USA.
[5]National Center for Atmospheric Research, Boulder, Colorado, USA.
[6]University Mayor de San Andres, La Paz, Bolivia.
[7]Howard University, Washington, District of Columbia, USA.
[8]University of Denver, Denver, Colorado, USA.
[9]Clarendon Laboratory, Oxford University, Oxford, UK.
[10]Langley Research Center, NASA, Hampton, Virginia, USA.
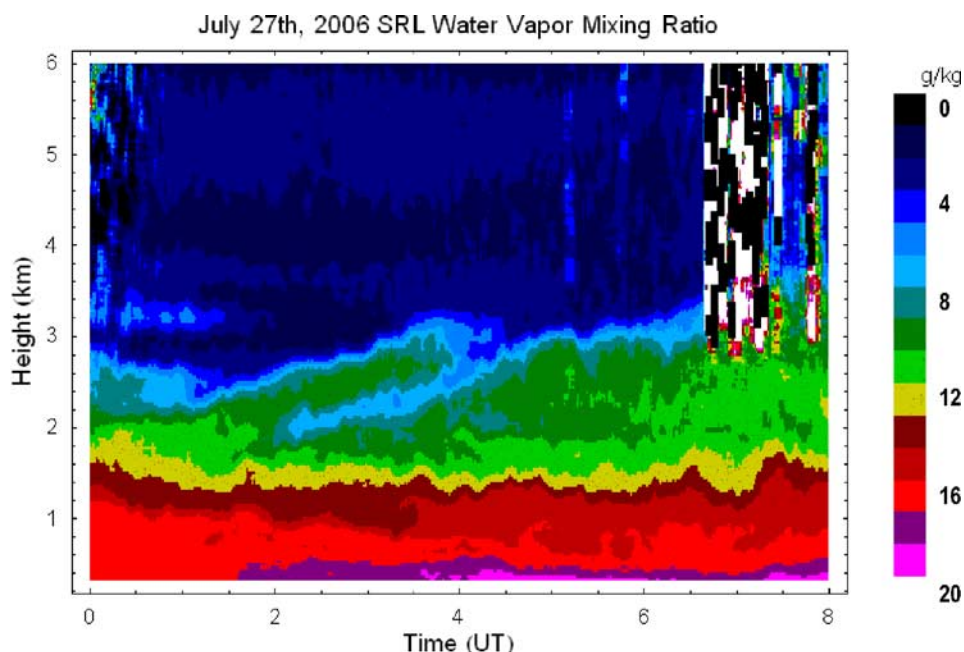[11]Raytheon Technical Services Company, Pasadena, California, USA.

Figure 1. Time series of water vapor profiles measured by a ground-based NASA/GSFC SRL lidar at Beltsville, Maryland, during WAVES_2006 on 27 July 2006. The lidar was colocated with the CFH launch site and the TES overpass time for this day was at 0718 UTC.

has traditionally been to improve numerical weather prediction (NWP) [*Smith*, 1991]. Providing water vapor profiles or spectral radiances for assimilation into NWP models is still the main objective of many current satellite sensors, for example the Atmospheric Infrared Sounder (AIRS) [*Tobin et al.*, 2006; *Divakarla et al.*, 2006]. However, for the Tropospheric Emission Spectrometer (TES), the requirement is to obtain the most likely state of the atmosphere within the field of view of the measurement. This applies whether water vapor is a tracer of air mass, of chemical interest, or whether it is an interferent. The central objective of TES is the measurement of global profiles of tropospheric ozone and its precursors, of which water is a key one. The accurate specification of water vapor can also be important in the measurement of other atmospheric trace gases and water vapor isotopes [*Worden et al.*, 2007]. For TES applications in which the objective is to map concentrations of chemical species, water vapor may be a spectral interferent that must be accurately specified to sense the species of interest (e.g., methane in the 1300 cm^{-1} spectral region). In this paper we compare the TES water vapor retrievals derived from spectral radiance measurements from TES [*Beer et al.*, 2001; *Beer*, 2006] with in situ sonde measurements.

[3] TES is an interferometric spectral radiometer flying on the NASA Aura platform (http://aura.gsfc.nasa.gov/ [*Schoeberl et al.*, 2006]). In the nadir-viewing mode, the mode appropriate to the validations described in this paper, the spectral radiometer has a resolution of 0.06 cm^{-1}. TES uses a 16 element detector array. Each detector has a 0.5 × 5 km nadir footprint at the surface, providing a total footprint of 8 × 5 km. The instrument has a number of observational modes (e.g., global survey, step-and-stare, transect). In global survey mode TES makes periodic measurements every ∼182 km along the satellite track; in step-and-stare mode nadir measurements are made every 40 km

along the track for approximately 50 degrees of latitude; in transect mode observations consist of a series of 40 consecutive scans spaced 12 km apart providing a coverage that is much more dense than the routine TES Global Survey viewing mode.

[4] In addition to the problem of making atmospheric measurements of water vapor with the required accuracy needed for satellite retrieval validations there is the challenging issue of the high spatial and temporal variability of atmospheric water vapor. This variability can cause dramatic sampling errors if the characterization of the atmosphere is not coincident in space with the field of view of the satellite instrument at the overpass time. Figure 1 shows a time series of water vapor concentrations obtained with the NASA/Goddard Space Fight Center (GSFC) Scanning Raman Lidar (SRL) stationed at the Howard University Research Campus at Beltsville, Maryland on 27 July 2006 as part of the Water Vapor Validation Experiment – Satellite/Sondes (WAVES_2006) initiative (http://ecotronics.com/lidar-misc/WAVES.htm). This day shows high variability, which is typical of atmospheric water vapor distributions. The magnitude of the variability makes it difficult to choose spatial and temporal coincidence criteria that would provide meaningful validations of satellite measurements with in situ sonde observations. The TES overpass is at ∼0700 UTC, a period in which sporadic cloud is in evidence.

[5] Many validations of water vapor retrievals rely heavily on profiles obtained from radiosonde measurements. Before describing a similar analysis for TES, we provide a perspective on the measurement capability of commonly used radiosondes. In conjunction with this analysis we consider the role of high-quality balloon-borne cryogenic frostpoint hygrometers (CFH). In addition to considering these techniques for characterizing profiles of atmospheric water vapor, we also address the implications of the associated

spatial and temporal sampling errors. The validity of ensemble statistics comparing retrieved and directly measured radiosonde profiles with their inherent error and sampling problems has severe limitations. Nevertheless it can be a useful exercise for qualitative comparisons and we include a sample of such results for TES.

[6] In order to validate satellite retrieved profiles and investigate any systematic differences there are four critical elements that must be evaluated: (1) the accuracy of the spectral radiometric measurements; (2) the quality of the forward model calculations; (3) the role of the retrieval procedure (e.g., impact of uncertainties in the retrieved cloud and temperature); and (4) the accuracy of the characterization of the radiating atmospheres used in the validation (e.g., measurement uncertainties and error that occur from different spatial and temporal sampling of the atmosphere). To provide insight into the roles of these elements we consider each of these in turn by performing radiance closure studies. In particular we look in detail at the spectral radiances from selected cases from the WAVES_2006 campaign.

2. Retrieval and Comparison Methodology

[7] The TES retrieval methodology is based on the maximum a posteriori estimate, which minimizes the difference between the observed spectral radiances and a nonlinear model of radiative transfer of the atmospheric state subject to the constraint that the estimated state must be consistent with an a priori probability distribution for that state [*Bowman et al.*, 2006]. In the TES retrieval, water vapor profiles are retrieved jointly with temperature and ozone. A priori profiles and covariances are calculated from the GEOS global transport model maintained at NASA's Global Modeling and Assimilation Office (GMAO) [*Bloom et al.*, 2005].

[8] If the estimated (retrieved) state is close to the actual state, then the estimated state can be expressed in terms of the actual state through the linear retrieval [*Rodgers*, 2000]

$$\hat{\mathbf{x}} = \mathbf{x}_a + \mathbf{A}(\mathbf{x} - \mathbf{x}_a) + \mathbf{Gn} + \mathbf{GK}_b(\mathbf{b} - \mathbf{b}_a), \qquad (1)$$

where $\hat{\mathbf{x}}$, $\mathbf{x}_a$, and $\mathbf{x}$ are the retrieved, a priori, and the "true" state vectors respectively. For TES trace gas retrievals, these are expressed as the natural logarithm of volume mixing ratio (VMR). The vector $\mathbf{n}$ represents the noise on the spectral radiances. The vector $\mathbf{b}$ represents the true state for those parameters that also affect the modeled radiance (e.g., concentrations of interfering gases, calibration, etc.). $\mathbf{b}_a$ holds the corresponding a priori values.. and the Jacobian, $\mathbf{K}_b = \partial\mathbf{L}/\partial\mathbf{b}$, describes the dependency of the forward model radiance, $\mathbf{L}$, on the vector $\mathbf{b}$. Further details on the TES forward model are provided by *Clough et al.* [2006]. The averaging kernel, $\mathbf{A}$, describes the sensitivity of the retrieval to the true state

$$\mathbf{A} = \frac{\partial\hat{\mathbf{x}}}{\partial\mathbf{x}} = \left(\mathbf{K}^T\mathbf{S}_n^{-1}\mathbf{K} + \Lambda\right)^{-1}\mathbf{K}^T\mathbf{S}_n^{-1}\mathbf{K} = \mathbf{GK}. \qquad (2)$$

$\mathbf{K}$ describes the sensitivity of the forward model radiances to the state vector ($\mathbf{K} = \partial\mathbf{L}/\partial\mathbf{x}$). $\mathbf{S}_n$ is the noise covariance matrix, representing the noise in the measured radiances, and Λ is the constraint matrix for the retrieval [*Bowman et*

al., 2006; *Kulawik et al.*, 2006a].$\mathbf{G}$ is the gain matrix, which maps from measurement (spectral radiance) space into retrieval space.

[9] For profile retrievals, the rows of $\mathbf{A}$ are functions with some finite width that gives a measure of the vertical resolution of the retrieval. The sum of each row of $\mathbf{A}$ represents the fraction of information in the retrieval that comes from the measurement rather than the a priori [*Rodgers*, 2000] at the corresponding altitude, providing the retrieval is relatively linear. The trace of the averaging kernel matrix gives the number of degrees of freedom for signal (DOFS) from the retrieval. An example of the sum of the rows of the TES water vapor averaging kernels during WAVES_2006 is plotted in Figure 5e, with the corresponding vertical resolution plotted in Figure 5f. The sensitivity of the TES retrieval may be affected by the signal-to-noise ratio (and therefore by the concentration of the trace gas of interest), by clouds and by the constraints used in the retrieval.

[10] The total error on the retrieved profile can be expressed as the sum of the smoothing error, the cross-state error, which accounts for errors due to other parameters in the joint retrieval (i.e., temperature and ozone), the measurement error (due to instrument random noise), and the systematic errors. An example of the estimated TES total error is plotted in Figure 5f. Full details of the TES retrieval error analysis are provided by *Worden et al.* [2004].

[11] There are a number of different ways to perform the comparisons between TES and in situ water vapor profiles, depending on the goal of the comparison. A comparison method that accounts for the a priori bias and the sensitivity and vertical resolution of the satellite retrievals is to apply the TES averaging kernel, $\mathbf{A}$, and a priori, $\mathbf{x}_a$. This method obtains an estimated profile $\mathbf{x}_{\text{in situ}}^{\text{est}}$ that represents what TES would measure for the same air sampled by the in situ measurements. A detailed outline of the procedure is provided in the TES Level 2 Data User's Guide [*Osterman*, 2006]. The TES standard procedure is to "map" the sonde data to the TES levels using a triangular convolution, but any preferred method could be used. The TES averaging kernel and the a priori are then applied to the mapped in situ profile:

$$\mathbf{x}_{\text{insitu}}^{\text{est}} = \mathbf{x}_a + \mathbf{A}_{xx}\left(\mathbf{x}_{\text{insitu}}^{\text{mapped}} - \mathbf{x}_a\right). \qquad (3)$$

[12] Differences between $\mathbf{x}_{\text{insitu}}^{\text{est}}$ and $\hat{\mathbf{x}}$ can then be presumed to be associated with the latter two terms in equation (1): the observational error on the retrieval or systematic errors resulting from parameters which were not well represented in the forward model (e.g., temperature, interfering gases, instrument calibration). The observational error is provided in the TES Level 2 data products. Note that differences between $\mathbf{x}_{\text{insitu}}^{\text{est}}$ and $\hat{\mathbf{x}}$ go to zero in regions where the TES retrieval contains little information from the measurement (is dominated by the a priori).

[13] There are other ways in which comparisons are commonly performed. For context we comment on them briefly in relation to the method used above. Occasionally comparisons are performed in which the retrieval sensitivity is ignored and the differences associated with retrieval systematic and random errors and those associated with
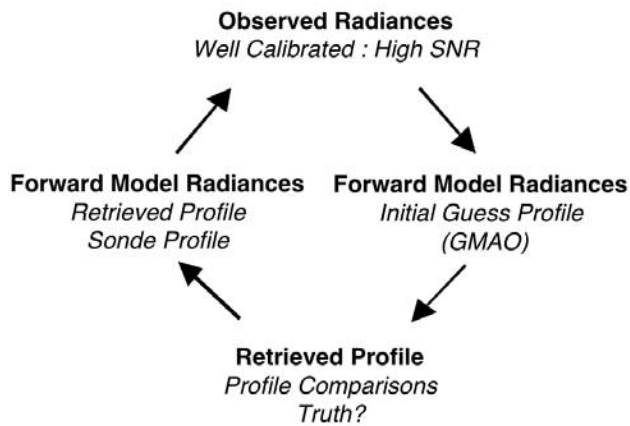
Observed Radiances
Well Calibrated : High SNR

Forward Model Radiances   **Forward Model Radiances**
Retrieved Profile   *Initial Guess Profile*
Sonde Profile   *(GMAO)*

Retrieved Profile
Profile Comparisons
Truth?

Figure 2. Schematic of a radiance closure study.

the a priori are grouped together. For this more simplistic brute force comparison method the sonde is smoothed according to the vertical resolution of the TES retrieval. The averaging kernels are normalized in order that the vertical resolution of the TES retrieval is accounted for in the comparison, but that the retrieval sensitivity is not. In reality, the vertical resolution and the sensitivity of the retrieval are connected, so this comparison should provide results similar to the previous method of applying the a priori and averaging kernel in regions where TES is sensitive. Another even more simplistic comparison method that is commonly performed is to ignore the sensitivity and the vertical resolution of the retrieval profile and just smooth both the high vertical resolution in situ data and the lower resolution TES retrieved state vector to some predefined standard altitude bins (e.g., 2 km). This smoothing can be done such that the total water column amount for both profiles is conserved. The result will show absolute differences between in situ and satellite measurements on some standard grid. However, these differences take no account of retrieval sensitivity or of the true vertical resolution of the retrieved parameter for the given conditions and thus provide no good way of distinguishing the reasons for the differences. Comparisons on a standard grid might be performed in order to try to relate different observations to one another (e.g., retrievals from different sensors). However, where possible more accurate comparison methods that utilize the sensitivity of both products, such as the intercomparison of remote sounding instruments method outlined by *Rodgers and Connor* [2003], should be used instead of a simple brute force comparison.

3. Radiance Closure Studies

[14] None of the profile comparison methods described above allow insight into the extent to which differences between TES and the in situ measurements are affected by the fact that the instruments may not be looking at the same air mass, which can often be the largest component of the differences under inhomogeneous conditions. Radiance closure studies are used to help separate the magnitude of the comparison difference due to sampling error (where the in situ observations are not measuring the same air mass as TES) from the component of the difference due to retrieval

performance, such as measurement uncertainties, forward model errors, and uncertainties in the retrieved temperature and clouds. All of these components must be evaluated in order to perform a comprehensive validation in which differences in the profiles comparisons can be investigated. Radiance closure studies are performed as follows and summarized in Figure 2.

[15] We start with observed radiances that are well calibrated with a high signal-to-noise ratio (SNR). A retrieval is performed that minimizes the variance between these observed radiances and forward model radiances, which start from an initial guess profile and are iterated to obtain a retrieved profile. At this stage the retrieved profile is then compared with an alternative profile measurement (e.g., radiosonde) that is considered as truth. In most validation studies, this is the point at which the comparison process stops. As noted above, the issue with this is that it is difficult to distinguish whether any observed differences in the profiles are due to sampling errors or systematic errors in the retrievals. To provide more insight, the forward model radiances are computed from both retrieved and sonde profiles and compared with the observed sensor radiances. If the retrieval converged then the residuals between observations and forward model calculations using the retrieved profile should primarily consist of random instrument noise. Information about the sampling error for the comparison can be obtained by comparing the residuals between the observed radiances and the forward model radiances generated from the comparison sonde profile. If the residuals are greater than the estimated systematic errors, then the sonde is not sampling the same atmosphere being observed by the sensor. Therefore, the magnitude of these residuals can be used to identify profile comparisons in which the sampling error contribution to the profile differences is small and the comparison constitutes a meaningful validation. In addition, since the same forward model is used to compute radiances from both the retrieved and sonde profiles, any systematic errors in the forward model will be mitigated by performing the differences of the differences between the observed forward model calculations.

4. TES Retrieval Comparisons With In Situ Measurements

[16] Presented are results from TES retrievals version V003, which are available from the NASA Langley Distributed Active Archive Center (DAAC). The main differences between V002 and V003 that influence the TES water vapor retrievals are: (1) improved TES temperature retrievals due to inclusion of the CO_2 $\nu2$ spectral region with improved CO_2 forward model calculations [*Shephard et al.*, 2008]; (2) the migration of TES initial guess and a priori from GEOS-4 to GEOS-5; (3) a lowered minimum value for the a priori cloud optical depth in order to better handle clouds with lower optical depths; and (4) the addition of more surface microwindows to help characterize the surface.

4.1. Radiosondes

[17] Radiosondes are launched frequently over a large part of the Earth's more populated regions and provide measurements that are often compared with satellite-retrieved water vapor profiles. There are several commonly

used radiosonde types [*Miloshevich et al.*, 2006]: the highly accurate CFH; the Sippican Mark IIa, used at 1/3 of the NWS (National Weather Service) sites, but not reliable at temperatures below −50°C; the Modem GL98 used at French overseas sites; and the Vaisala sondes, the most widely deployed sondes in the U.S. and at American overseas sites. The Vaisala RS80-H is frequently used at NWS sites, while the Vaisala RS92, the most recent Vaisala radiosonde model, is currently used at ARM (Atmospheric Radiation Measurement) program sites.

[18] Radiosonde profiles are often considered "truth", but inconsistency between measurements by different types of profilers, or even in profiles recorded by the same type of instrument, have been repeatedly noted [*Cady-Pereira et al.*, 2008; *Turner et al.*, 2003, and references therein]. Determining the source of these inconsistencies and developing methods to remove them has been the focus of much research in recent years. In order to provide some perspective on the issues encountered we will briefly discuss the Vaisala series.

[19] Comparisons of thousands of sonde total column precipitable water vapor (PWV) measurements with PWV retrievals from a MWR (Microwave Radiometer) showed that RS80 profiles have a significant dry bias during both day and night [*Turner et al.*, 2003]. In addition, the daytime RS90/92 radiosonde PWV is typically 3% to 8% higher than the nighttime factor when compared with the MWR [*Miloshevich et al.*, 2006]. The daytime dry bias has been attributed to solar heating of the sensor. An empirical temperature and pressure-dependent correction based on the CFH was developed for the set of RS92s examined by *Vömel et al.* [2007a], which when applied to the RS92 profiles greatly reduced the difference with respect to the CFH (∼7% up to ∼15 km). However, this empirical correction depends on latitudes, solar zenith angles, etc., limiting its applicability to other regions. *Cady-Pereira et al.* [2008] have developed a simple semiempirical correction to the radiosonde total column water vapor that is a function of the solar zenith angle and effectively removes the daytime dry bias in the total column PWV. They also show that for nighttime observations, combining the within batch and between batch variability can result in differences between radiosonde total column PWV measurements as large as 18%. Scaling the sonde profile by the MWR PWV value can help correct the total column PWV but does not resolve errors in the upper troposphere.

[20] Two other problems are particularly significant for researchers interested in the upper troposphere, where the environment is colder and drier. First, all water vapor profilers are subject to "time-lag" (TL) error due to the finite response time to changes in ambient humidity [*Miloshevich et al.*, 2006]. Time-lag error changes the shape of the profile in the middle and upper troposphere and has the greatest impact where there are steep humidity gradients (e.g., above and below cirrus clouds, at the tropopause). *Miloshevich et al.* [2004] developed a time-lag correction algorithm for the Vaisala radiosondes. Deficiencies in the Vaisala calibration models at lower temperatures have led to the development of "temperature-dependent" (TD) corrections, which can be as large as 32% at −80°C for the RS80 [*Miloshevich et al.*, 2006]. TD corrections are also available for the RS90 and RS92 sensors, but changes in calibration

and design since the inception of these sensors demand that these corrections be applied with caution. For the AWEX-G campaign, *Miloshevich et al.* [2006] derived empirical calibration corrections for the Vaisala profilers with respect to the CFH measurements. A similar procedure was carried out during the Ticosonde campaign [*Vömel et al.*, 2007a] and the WAVES_2006 campaign. The reported measurement uncertainties of the CFH itself depend on altitude and are less than 4% in the tropical lower troposphere, 9% in the tropopause region, and 10% in the middle stratosphere (∼28 km) [*Vömel et al.*, 2007b]. Presently this is not a methodology that is practical for operational data collection, but it can provide accuracy estimates.

[21] Comparisons of CFH and Vaisala RS92 soundings show that, compared to the CFH, the RS92s have an average daytime systematic dry difference on the order of 9% at the surface that increases with altitude and can reach 50% near the tropopause (∼15 km) [*Vömel et al.*, 2007a]. Nighttime comparisons of CFH and Vaisala RS92 show smaller dry bias than during the daytime [*Miloshevich et al.*, 2006]. These comparisons in the lower troposphere have a bias typically of ∼1−5% (with a maximum of 13% with relative humidity between 5 and 10%) and standard deviations of ∼3−7% (with a maximum of 23% for relative humidity between 5 and 10%) [*Miloshevich et al.*, 2006]. In the upper troposphere for relative humidity decreasing from 60% to 5%, the typical dry bias and standard deviation increase to ∼7−11% and ∼14−51%, respectively.

[22] In summary, radiosondes provide an estimate of the atmospheric water vapor profile. The quality of this estimate can be improved by carefully applying corrections. Calibration corrections are very dependent on the "batch" of the instrument, but are certainly necessary for rigorous validation of satellite remote sensing algorithms, which are sensitive to the structure of the water vapor profile in the upper troposphere.

4.2. Global Comparisons of TES Water Vapor Retrievals With Vaisala Radiosondes

[23] Results from TES water vapor retrieval comparisons with global distributed National Weather Service's Centers for Environmental Prediction (NCEP) Vaisala RS90 and RS92 radiosondes are presented in Figure 3. The coincidence criteria for matches between radiosonde launches and TES overpasses is within 1 h and 100 km. Only the more accurate nighttime radiosonde measurements are used in the comparison. We also screened the comparisons based on the TES quality flag and the TES water vapor sensitivity (sum of the rows of the averaging kernel ≥ 0.70). A subset of comparisons where the TES cloud effective optical depths are less than or equal 0.1 is also provided in Figure 3. TES comparisons for the full ensemble of cases have a mean differences of <5% and a standard deviation of ∼20% in the lower troposphere (below ∼600 hPa) with the radiosonde being drier. This TES moist bias compared with the sonde observations increases to a maximum of ∼15% in the upper troposphere between ∼300−200 hPa. The standard deviation in this region reaches ∼40%. The TES comparison in Figure 3 with reduced cloud influence shows similar results to the set with clouds included. This is a reasonable result as points where TES has low sensitivity were removed from the statistics (i.e., regions below optically thick clouds). The
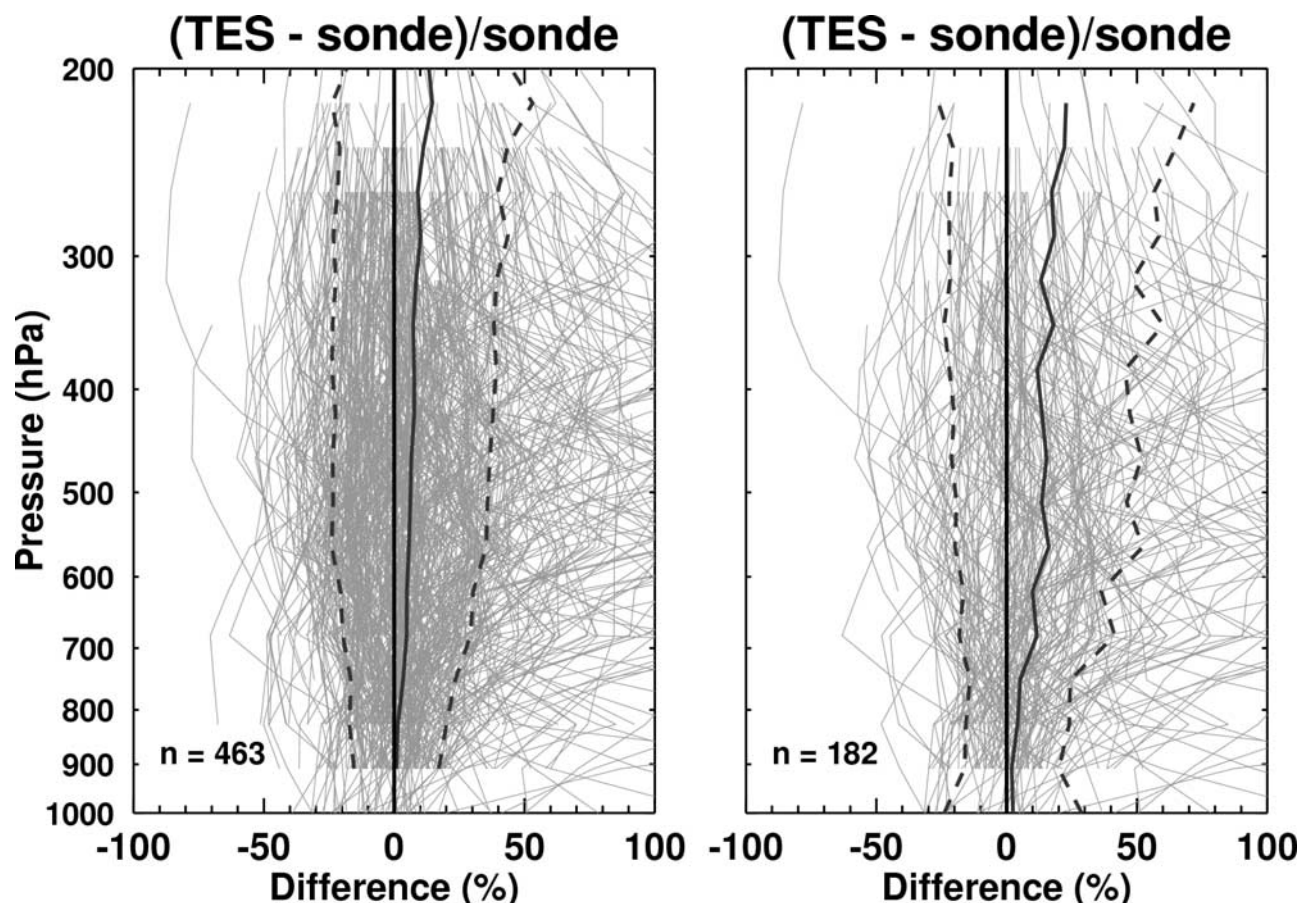
Figure 3. Global comparisons of TES V003 water vapor profiles with the Vaisala RS90 and RS92 radiosondes from NCEP. The coincidence criteria are within 100 km and 1 h of a TES overpass. Only nighttime profiles are included. The black solid lines are the mean differences, and the dotted lines are the 1-sigma standard deviation. The gray solid lines are all the individual comparisons. Similar plot containing a subset of the comparisons where the TES effective cloud optical depth is less than or equal to 0.1.

percent difference comparison values in Figure 3 are plotted as a function of the level water vapor volume mixing ratio (VMR) values in Figure 4. Note that any points outside the 3-sigma standard deviation line plotted in Figure 4 were marked as outliers and not used in computing the standard deviation values in either Figure 3 or Figure 4. This scatterplot shows that in general the relative percent differences increase with decreasing water vapor VMR. This is reflected in the larger errors in the upper troposphere of Figure 3 where the water vapor values tend to be small.

[24] It is difficult to utilize these global TES/radiosonde comparison results to provide detailed validation of the TES retrievals as there is no real "truth" due to errors in the global uncorrected Vaisala RS90 and RS92 radiosondes. As stated in section 4.1, nighttime radiosonde total column PWV measurements have combined within batch and between batch variability as large as 18%. Also, in the lower troposphere under conditions in which the relative humidity is greater than 10%, simultaneous comparisons of Vaisala RS92 with CFH measurements show nighttime bias and standard deviations of $\sim$1–5% and $\sim$3–7%, respectively. In the upper troposphere for relative humidity decreasing from 60% to 5%, the typical dry bias and standard deviation increase to $\sim$7–11% and $\sim$14–51%, respectively. In addition, there are

inherent sampling errors by comparing point source observations with satellite observations that are often not observing the same air mass. As pointed out in the introduction this is especially true for water vapor, which typically is variable over short time periods and distances in the atmosphere (e.g., see Figure 1).

[25] Given some of the similarities TES and AIRS share (nadir-viewing, infrared sensors, flying on polar orbiters just 15 min apart), it is common to compare the TES radiosonde comparison results with those from AIRS validation exercises. AIRS and TES both provide water vapor profile retrievals; however, the objectives of the TES and AIRS missions are very different. AIRS' primary objective is to provide water vapor profiles or spectral radiances for assimilation into numerical weather prediction and GCM models. For this purpose there is a rationale for having the AIRS forward model and associated adjoint model consistent with radiosonde profiles [*Strow et al.*, 2006]. TES is designed to improve our knowledge of atmospheric chemistry, and thus seeks to characterize the most likely atmospheric state within the TES field of view (FOV). This applies whether water vapor is a tracer of air mass, of chemical interest, or whether it is an interferent. The TES effort has been focused on in-depth radiative closure exercises carried out on case
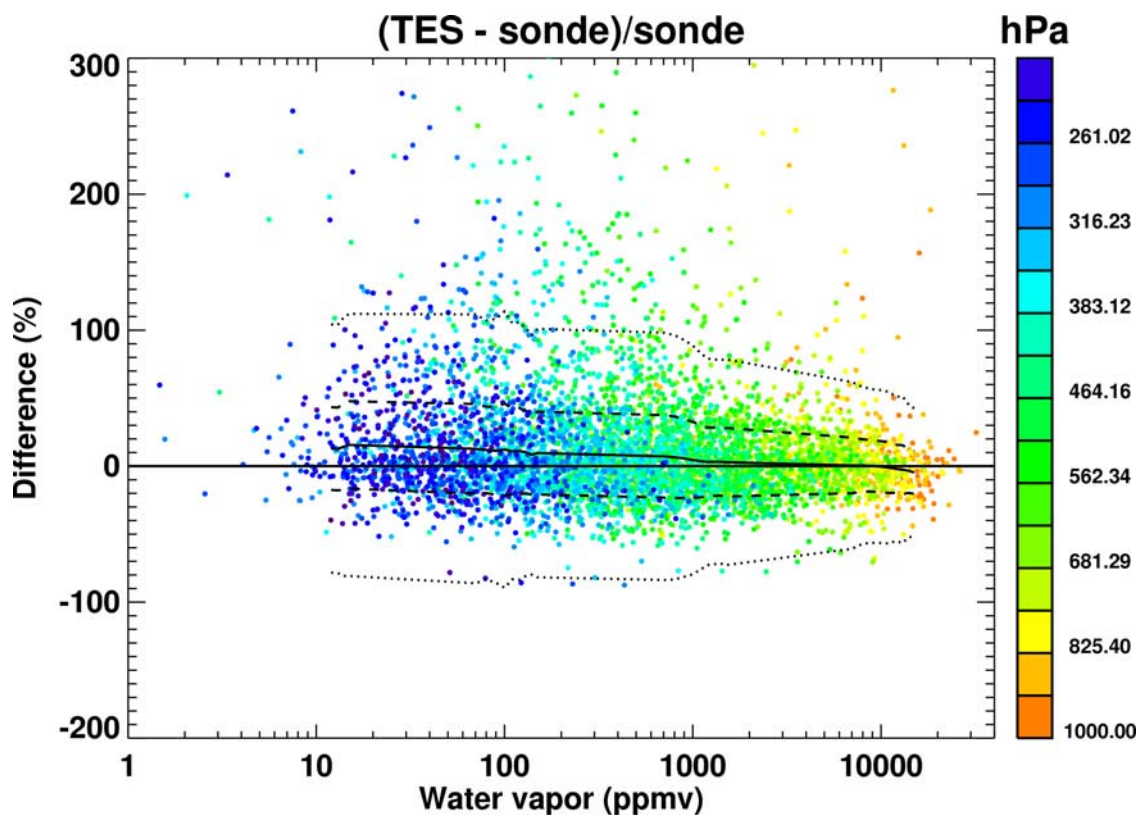
Figure 4. Scatterplot of the percent differences shown in Figure 3 as a function of level volume mixing ratio.

studies in which the forward model has not been specifically tuned with radiosonde profiles. In normal operational mode TES points down in the nadir whereas AIRS provides more coverage by scanning, which provides many more opportunities for matchups with radiosondes. These differences in coverage and purpose must be kept in mind when comparing the results of the validation exercises.

[26] *Tobin et al.* [2006] carried out an AIRS validation effort by reducing as much as possible the sources of differences between AIRS retrieved profiles and sonde profiles, using ARM best estimates of the atmospheric state during three long sets of approximately 90 AURA overpasses at the ARM SGP and TWP sites. ARM best estimates of the water vapor profiles were obtained using pairs of Vaisala RS-90 sondes launched around the AIRS overpass time; profiles were "microwave scaled", and temporally and spatially interpolated to the overpass time and location. Mean and root-mean-square (RMS) percent differences between the AIRS and sonde profiles were then computed following the convention for reporting AIRS statistics [e.g., *Susskind et al.*, 2003], where the observed differences were weighted by the layer water vapor amounts, independently for each layer. This procedure reduces the effect of typically higher percentage errors at low water vapor amounts, which has greater impact in regions of larger water vapor variability such as in the lower troposphere at SGP. *Tobin et al.* [2006] reports that this water vapor weighting reduced mean bias from 20% to ~5% and the RMS differences from 55% to 20% in the lower troposphere at the ARM SGP site.

[27] *Divakarla et al.* [2006] took the approach of comparing a very large number (over 82000) of AIRS retrieved profiles from around the globe with unadjusted profiles measured by a variety of profiling instruments. The criterion for collocation was ±3 h of time coincidence and less than 100 km between the center of the AIRS footprint and the sonde location. The sonde profiles were used as measured, without any of the spatial, temporal and total column adjustments applied by *Tobin et al.* [2006]. The reported AIRS global RMS values ranged from 20% to 45%; however, it is important to note that these value were also computed using the AIRS convention of weighting the differences by the water layer vapor amounts, which as previously stated leads to significantly lower computed mean and RMS values in sets that contain large water vapor variability [*Tobin et al.*, 2006].

[28] The TES global validation described above included ~450 unadjusted sonde profiles. Since this is a global profile set no corrections were available that could be applied to the radiosonde profiles to improve their measurement accuracy. Obtaining a larger number or adjusting the radiosonde profiles would provide more accurate comparisons. Moreover, no weighting was applied to the TES-sonde differences. It is expected that applying a weighting to the differences would significantly decrease the TES reported statistics, as it does for AIRS. However, since the TES central objective is to provide the most likely state of the atmosphere within the FOV of the TES measurement, we are interested in comparisons results under all conditions. Therefore, we do not wish to empirically tune the
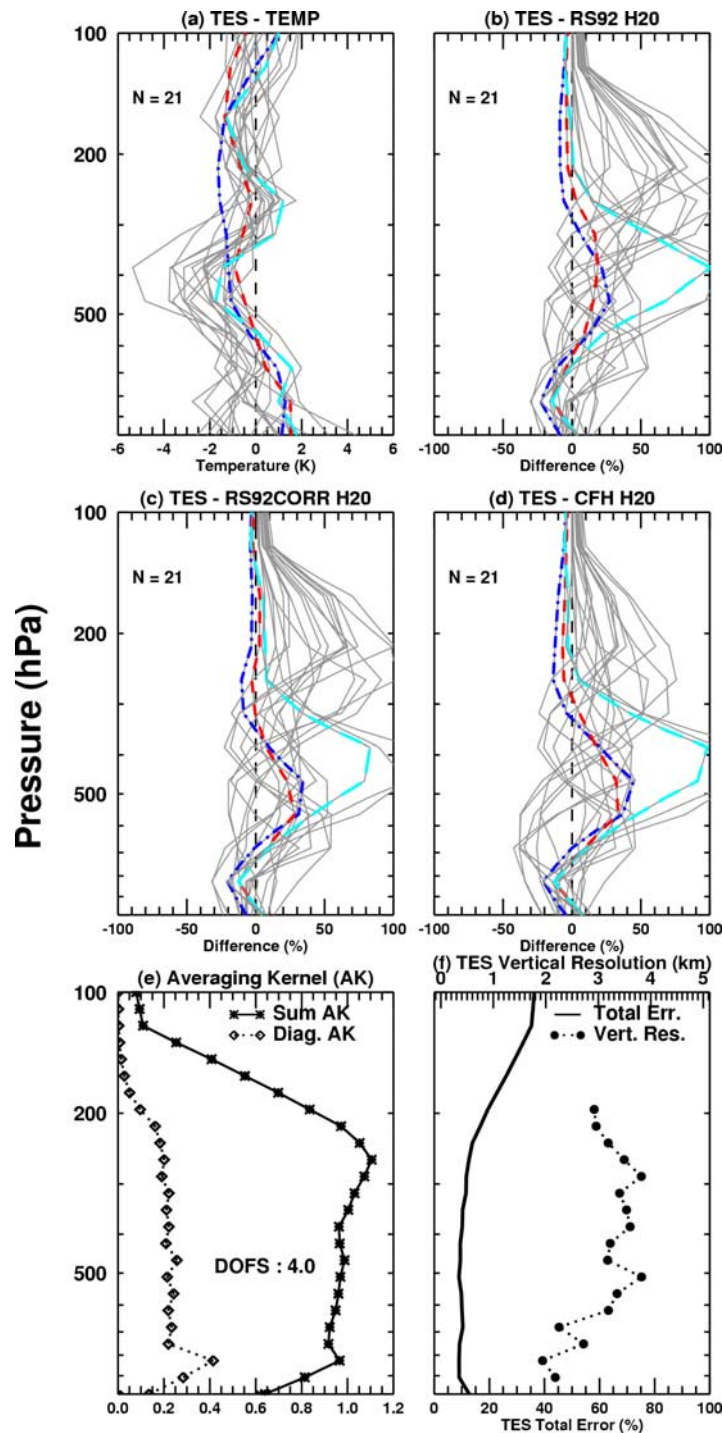
Figure 5. TES V003 comparison with sondes during WAVES_2006. The comparison consists of 21 nighttime matchups that have a coincidence criteria of 60 km and 1.5 h. Figures 5a–5d compare the TES retrievals with the sondes. (a) The RS92 temperature comparison, which is included for the purpose of determining its impact on the water vapor retrievals. (b) The water vapor comparisons with the RS92, (c) the RS92 with an empirical correction applied on the basis of the CFH, and (d) the CFH. TES run 4803, sequence 1, scans 19, 20, and 21 that are presented in the radiance closure study are highlighted in blue (dashed-dotted line), red (short dashed line), and cyan (long dashed line), respectively. (e) The median value of the diagonal of the averaging kernels and the sum of the rows of the averaging kernels of all 21 cases. The total degrees of freedom for signal (DOFS) is also labeled on Figure 5e. (f) The median value of the estimated TES total error generated from the square roots of the diagonal elements in the output total error covariance matrix, which includes systematic errors, measurement errors, and retrieval smoothing errors. Figure 5f also contains the vertical resolution of the TES water vapor retrieval plotted as a function of pressure, which is computed from the full width at half maximum of the rows of the averaging kernels.
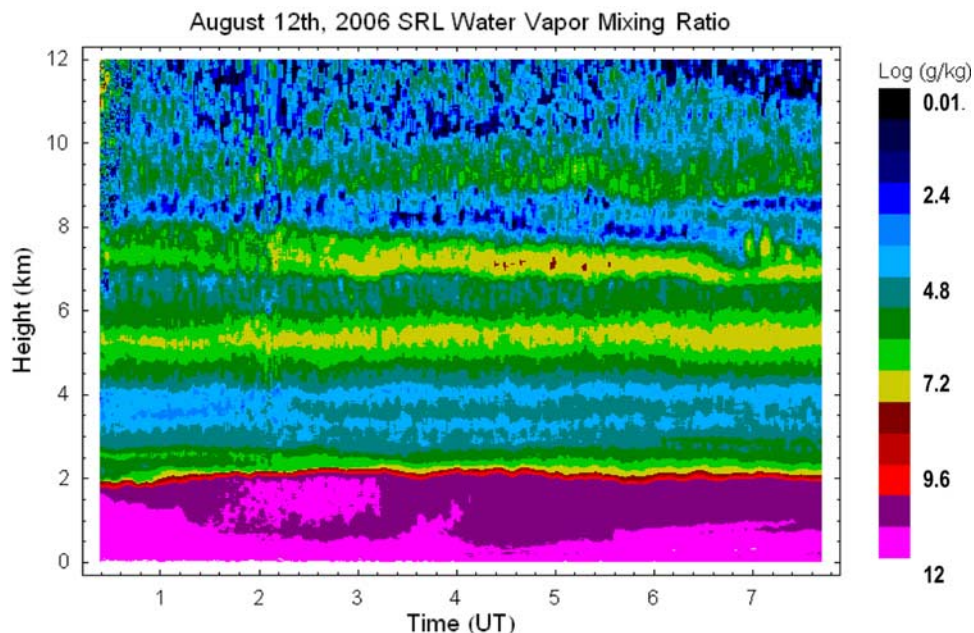
Figure 6. Time series of water vapor profiles measured by a ground-based NASA/GSFC SRL lidar at the WAVES site on 12 August 2006. The CFH launch site was colocated with the lidar and was launched at 0601 UTC. The TES overpass was at 0719 UTC.

absorption coefficients in the forward model to provide better agreement with radiosondes or perform the statistics that tend to weight out the potentially interesting low water vapor cases that have larger relative percent differences. With these caveats, the mean TES/radiosonde global comparison differences ranging from 5% to 10% and corresponding standard deviations of 25% to 45% between 1000 and 400 hPa are comparable with AIRS [*Tobin et al.*, 2006] reported unweighted mean of 20% and RMS of 55% obtained at ARM SGP.

[29] Without additional information the conclusions that can be drawn about the performance of the TES water vapor retrieval from this type of general profile comparison of retrievals with radiosondes are limited as it difficult to analyze the potential causes for the comparison differences (e.g., measurement uncertainties, forward model error, retrieval errors, sampling errors, etc.). In order to carry out a detailed validation of the TES water vapor retrievals, which would obtain the most likely state of the water vapor field within the field of view of the TES observations, rather than a simple comparison, further steps have to be taken in order to characterize the systematic errors and ensure that the TES/sonde sampling error is minimized in the comparisons. The following section describes detailed comparisons where other coincident water vapor observations and radiance closure studies are used to select comparisons with sondes that better represent the true air mass being observed by TES.

4.3. Detailed Comparisons of TES Water Vapor Retrievals With Sondes

[30] In order to investigate the TES retrievals further we focused on water vapor measurements made during the WAVES_2006 campaign. During WAVES_2006 sondes were launched so that they were coincident and colocated with TES-Aura overpasses. To ensure better coincidences during this intensive water vapor measurement period, TES

performed special observations in Transect viewing mode over the WAVES_2006 Beltsville, Maryland, US, site every other day. These Transects scans are spaced 12 km apart providing coverage that is much more dense than the routine TES Global Survey viewing mode. During this experiment Vaisala RS92 humidity sensors and the CFH were flown on the same balloon. This facilitated the comparison between the Vaisala RS92 and the CFH and the derivation of *Miloshevich et al.* [2004, 2006] RS92 empirical correction. During WAVES there were 21 TES nighttime overpasses that were within 60 km and 1.5 h of a CFH launch. Figure 5 shows the comparison results for the 21 cases with TES V003. The TES/RS92 comparisons are similar to the global NCEP comparisons in Figure 3. TES/ CFH comparisons are better in the upper troposphere (~300 hPa to the tropopause) than the TES/RS92 comparisons, which is expected since the CFH provides more accurate observations in the upper troposphere. However, the comparison differences between the TES water vapor retrievals and the sonde observations are generally large. To investigate this further, comparisons were selected from WAVES_2006 for radiance closure studies.

[31] On 12 August 2006 there was a CFH launch at 0601 UTC and a TES Transect overpass 1 h and 18 min later at 0719 UTC. TES Run 4803, Sequence 0001, scan 20 is selected as it was 0.45 km from this balloon launch site. For comparison purposes we also selected the two adjacent TES scans (scan 19 and scan 21), which are 12 km to either side of scan 20 along the transect. The three selected scans are highlighted in Figure 5. This time period was chosen because the time series of lidar profiles at the Beltsville, Maryland, site, shown in Figure 6, indicates that the water vapor variability for this day is relatively stable. For example, compare this plot with the lidar profile time series from 27 July 2006 (Figure 1). These scenes were also selected because they are virtually cloud free, which limits
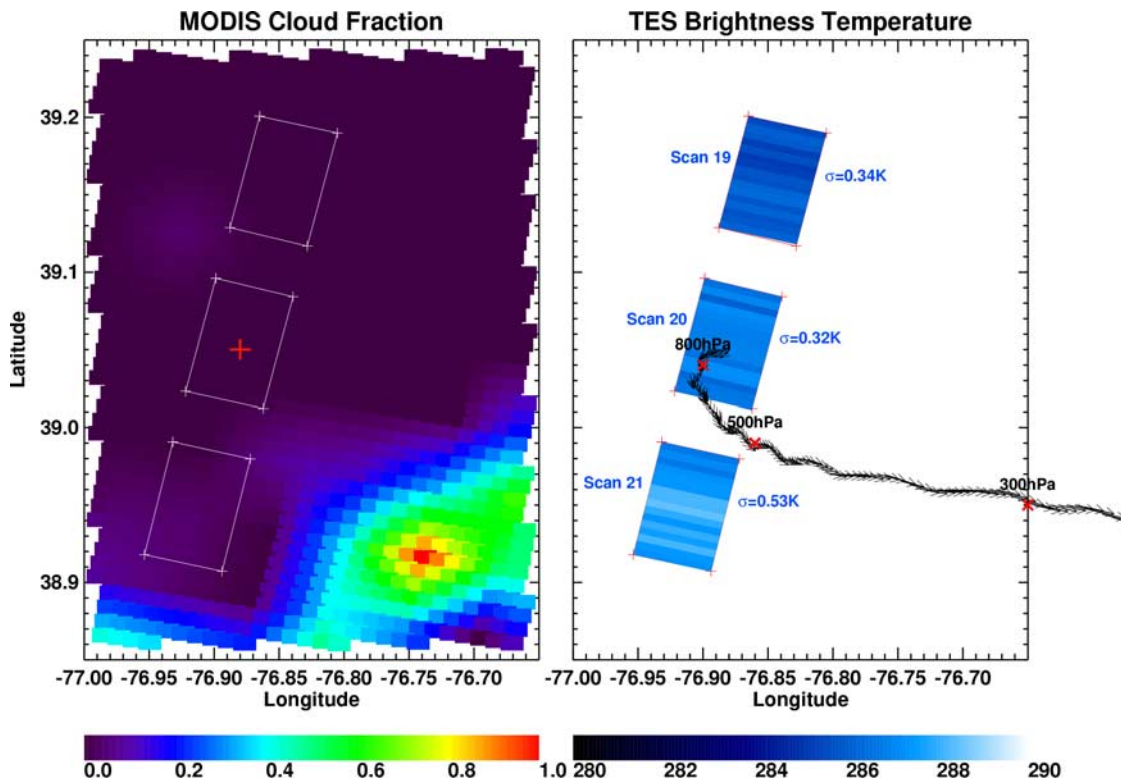
Figure 7. (left) The MODIS 1 km cloud fraction on 12 August 2006 at 0700 UTC over the WAVES_2006 Beltsville, Maryland, site (marked by the red cross). Overplotted on the cloud mask are the TES footprints from scans 19, 20, and 21. (right) The TES surface brightness temperatures at 1105 cm^{-1} from the 16 (0.5 × 5 km) pixels within the TES three scans. Also, overplotted on the plot is the flight path of the sonde with selected altitudes indicated by red crosses.
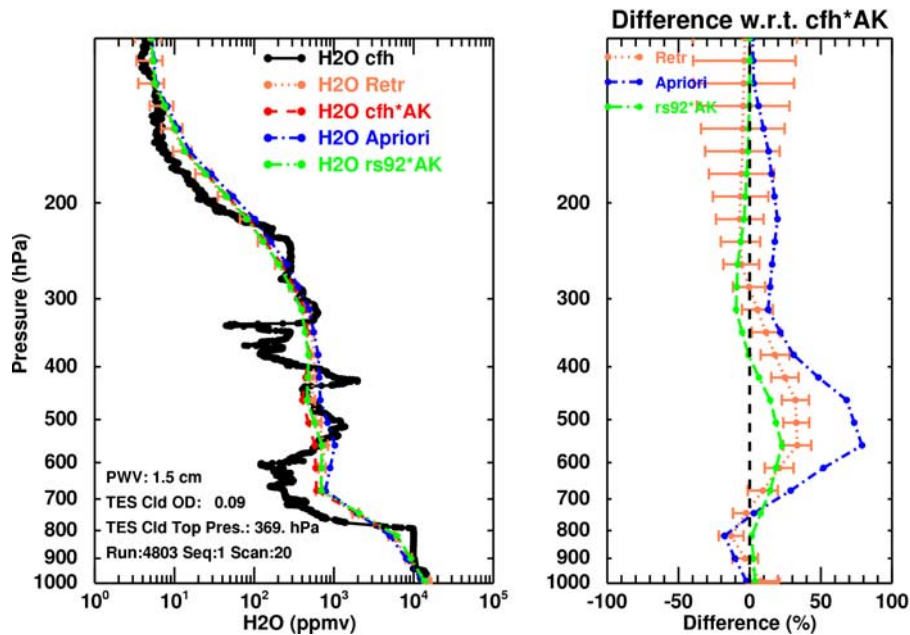
Figure 8. This is a CFH comparison plot on 12 August 2006 that corresponds to TES scan 20. The CFH launch was launched 12.5 km away and 1 h and 17 min before this TES scan. (left) The observed CFH profile (black), the a priori profile (GMAO) (blue), the TES retrieved profile (salmon), and the CFH (red) and RS92 (green) profiles with the TES a priori and averaging kernels (AK) applied. (right) The relative percent differences (Profile − CFH/CFH) × 100 of the different profiles with respect to the CFH with the TES a priori and averaging kernel applied (dotted line at zero).
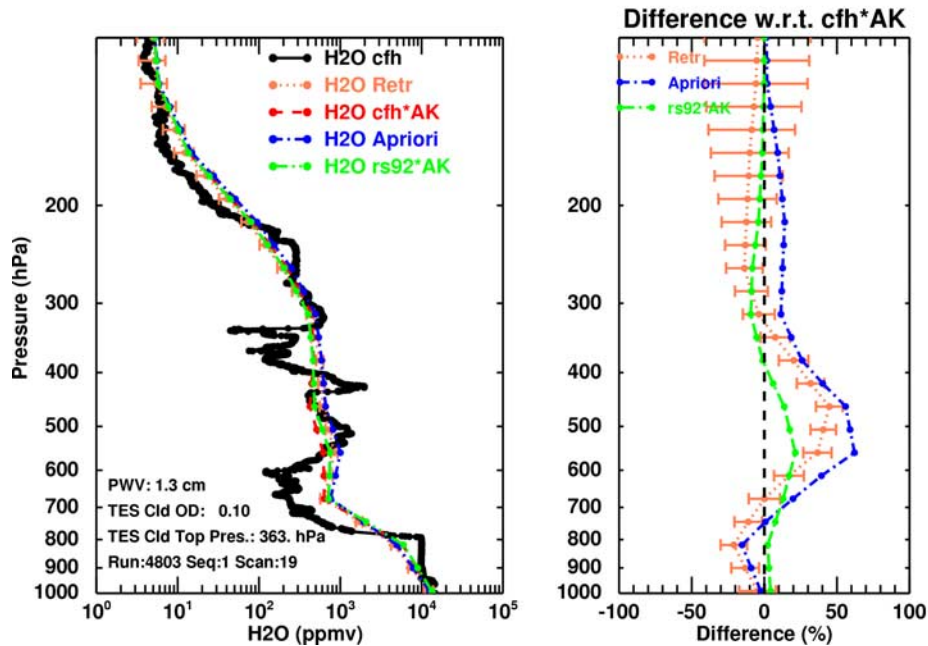
Figure 9. Same as Figure 8 but for TES scan 19.

the impact of the clouds on the comparisons. The Moderate Resolution Imaging Spectroradiometer (MODIS) 1 km cloud fraction in Figure 7 indicates that there are no clouds in scans 19 and 20 and that there is less than 5% cloud cover in any of the 1 km MODIS pixels for scan 21. The ground based lidar measurements (not shown) indicate that there were intermittent cirrus clouds between 10 and 13 km over the Beltsville site; at the time of the TES overpass (0719 UTC) there were no lidar observations of clouds,

but there were lidar measurements of cirrus clouds at ∼0650 and 0730 UTC with estimated cloud optical depths at 355 nm of less than 0.2. Another metric that can be used to provide information on whether clouds are present in a TES scan is the interpixel surface brightness temperature variability of the 16 pixels that comprise a scan. The reasoning follows that if a cloud is present in a TES pixel then its radiating properties will be much different than the surface and the 16 pixels will be inhomogeneous. The standard
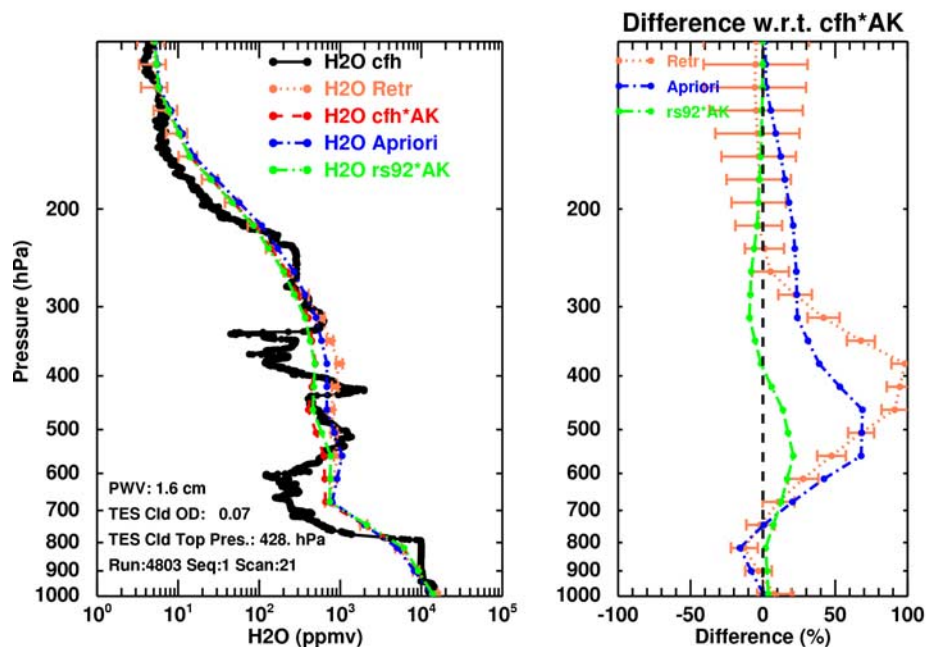

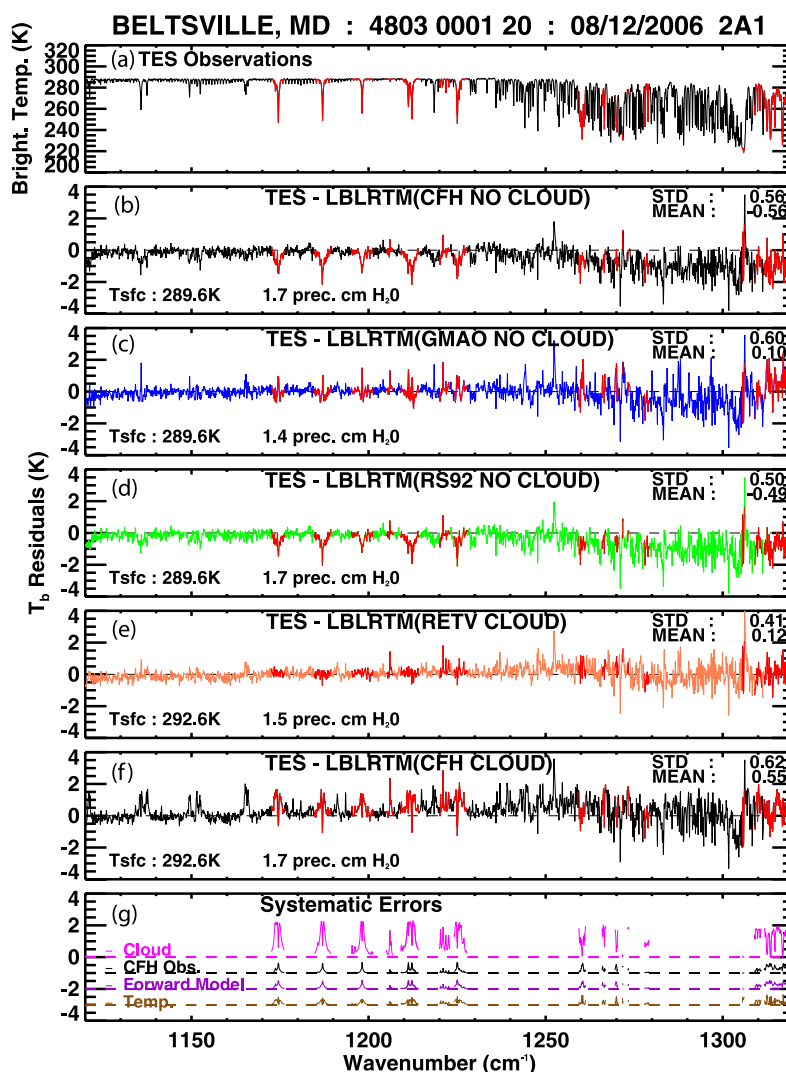**Figure 10.** Same as Figure 8 but for TES scan 21.

Figure 11. Radiance closure study for the WAVES_2006 comparison on 12 August 2006 of sondes with for TES scan 20. The red lines indicate the microwindows where the TES retrieval was performed. (a) Plot of the observed TES spectrum. Plots of (b) TES – LBLRTM calculated spectrum using the CFH specified atmosphere with no clouds, (c) TES – LBLRTM calculated spectrum using the TES a priori (GMAO) specified atmosphere with no clouds, (d) TES – LBLRTM calculated spectrum using the RS92 specified atmosphere with no clouds, (e) TES – LBLRTM calculated spectrum using the TES retrieved atmosphere including cloud optical depths, and (f) TES – LBLRTM calculated spectrum using the CFH atmosphere including TES retrieved cloud optical depths. (g) Contributions in the TES microwindows from estimates of systematic errors in the retrieved cloud optical depths, uncertainties in the CFH observations (plotted with a −1 K offset), forward model water vapor calculations (plotted with a −2 K offset), and retrieved temperature profile (plotted with a −3 K offset).

deviation of the brightness temperatures in the atmospheric window at 1105 cm^{-1} for the 16 pixels across the scans is very small (scan 19 = 0.34 K, scan 20 = 0.32 K, and scan 21 = 0.53 K), especially when you consider these scans are over land, which in general does not have a homogeneous background surface. Also shown in Figure 7 is the flight path of the CFH used in the comparison, which was launched about 1 h before the MODIS overpass and 1 h and 18 min before the TES overpass. This demonstrates that a sonde can drift significantly from the launch site during ascent making it challenging to compare balloon-borne in situ profiles with instantaneous satellite retrieval

profiles, even if the sonde launch site and the overpass footprint are colocated.

[32] Figures 8–10 contain profile comparisons of the TES retrieved profile, the a priori (GMAO), and the RS92 with the CFH for scan 20 and its two adjacent scans 19 and 21, respectively. Since the goal of this study is to validate TES retrievals, the TES averaging kernels and a priori were applied to the sondes (see equation (3)). The range in the magnitude of the peak profile differences between the CFH and the three TES scans, which are only 12 km apart, go from ∼35% to 100% around the middle of the troposphere (∼500 hPa). A radiance closure analysis is performed for these three cases to provide more information on the differences.
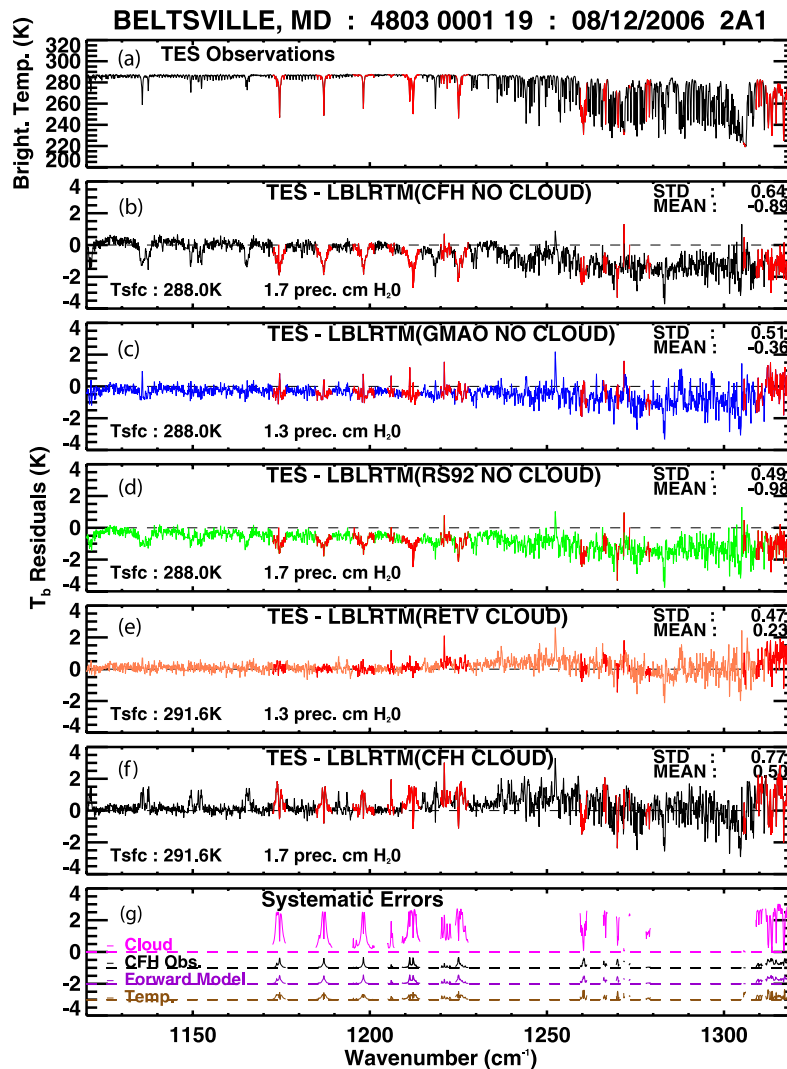
Figure 12. This figure shows the radiance closure study for the WAVES_2006 comparison on 12 August 2006 for TES scan 19 using the same plotting convention as Figure 11.

[33] The Line-By-Line Radiative Transfer Model (LBLRTM) is the forward model used by TES [*Clough et al.*, 2005, 2006]. LBLRTM was used to calculate radiances from the CFH, a priori (GMAO), RS92, and TES retrieval profiles. All the radiances were converted to brightness temperatures. Figures 11–13 show the radiance closure study for scans 20, 19 and 21, respectively.

[34] We will first discuss the radiance closure study for scan 20 (Figure 11) since its footprint encompasses the launch site of the CFH. The highlighted red areas are the spectral regions to focus on in Figures 11–13 as they are the TES microwindows used in the retrievals. The brightness temperature residuals corresponding to the profiles being compared in Figure 8 are shown in Figures 11–13 (b–e). Since the MODIS cloud fraction, the TES interpixel variability, and the lidar profiles suggest that there were no detectable clouds during the time of the TES overpass, the radiance calculations for the sonde profiles in Figures 11–13 (b–d) were computed assuming there were no clouds. An important goal of these closure studies is to determine how well the sonde profiles sampled the true atmospheric state being observed by TES. If the sonde sampled the true

atmospheric state being observed by TES then the brightness temperature residuals (TES observations–forward model calculations) would be no larger than the radiance contribution from the combined systematic errors from the forward model, TES instrument errors, the sonde water vapor and temperature measurement errors, and the cloud retrieval errors (if present). Negative (TES-sonde) brightness temperature residuals in the water vapor lines greater than the systematic errors indicate that there is not enough water vapor in the part of the profile corresponding to that spectral region. Conversely, positive residuals indicate that there is too much water vapor at these levels. Assuming that there are no clouds, the contribution to the brightness temperature residuals from the systematic errors due to uncertainties in the CFH measurements [*Vömel et al.*, 2007b], the forward model error [*Rothman et al.*, 2003; *Gordon et al.*, 2008; M. W. Shephard et al., manuscript in preparation, 2008], and temperature retrieval errors (refer to Figure 5a and the more detailed analysis by R. L. Herman et al. (manuscript in preparation, 2008)) are of the order of half a degree each (see Figure 11g). The TES instrument measurement systematic error is determined from TES
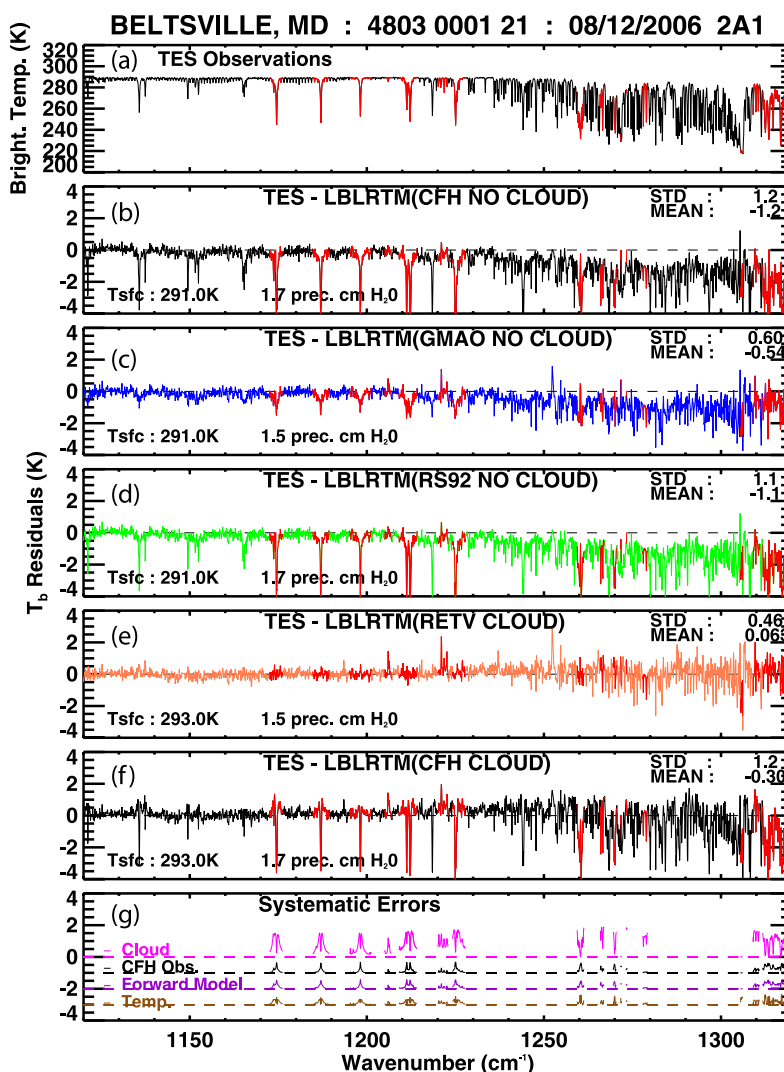
Figure 13. This figure shows the radiance closure study for the WAVES_2006 comparison on 12 August 2006 for TES scan 21 using the same plotting convention as Figure 11.

radiance validations [*Shephard et al.*, 2008] and shown in Figure 14 to be on the order of tenths of a degree Kelvin. Note that it is difficult to compute a total systematic error value at this stage as the extent of the interdependence of the systematic errors is not known. (i.e., the systematic errors can only be additive if they are independent). However, even if all these errors were independent and additive then an estimate of the total systematic error would be on the order of ∼1.0 K (center of the water vapor lines).

[35] The negative residuals in Figure 11b are a little larger than the estimated total systematic errors, which indicates that the CFH is a little drier than the atmosphere being observed by TES. The scatterplot in Figure 15 suggests that the larger brightness temperature residuals of ∼2 K correspond to the middle troposphere (∼500 hPa), which are where the profile differences in Figure 8 are the largest compared with the CFH. The positive residuals in Figure 11c for the a priori (GMAO) profile are larger than the systematic errors, indicating that there is too much water vapor in the middle to upper troposphere levels of the profile. The small residuals from the spectral regions with the signal

coming from the lower part of the troposphere (greater than ∼800 hPa) indicate that the a priori profile agrees well with the TES observations in this part of the atmosphere. The negative residuals in Figure 11d for the RS92 are a little smaller than the CFH, which shows that in this case the RS92 is a little closer to sampling the atmosphere being observed by TES. The magnitude and sign of brightness temperature residuals in Figure 11 (b–d) are greater than the estimated total systematic errors and are consistent with profile differences between the TES retrieved profile and the other sondes. This suggests that the large profile comparison differences are likely due to the fact that the sondes are not sampling the same air mass as TES. Figure 11e shows the residuals obtained by comparing the TES observations with the calculated radiances generated using the TES retrieved profile. This demonstrates that the TES retrieval was effective in minimizing the residuals.

[36] The TES retrieved effective cloud optical depths are reported spectrally [*Kulawik et al.*, 2006b; *Eldering et al.*, 2008] with an average value of 0.09 at a cloud top pressure of 369 hPa for scan 20. This high altitude, optically thin
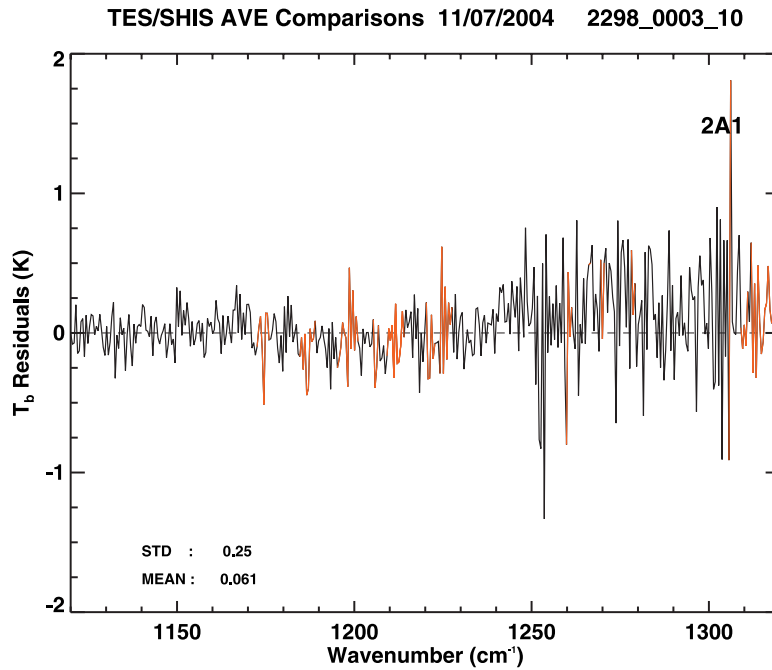
Figure 14. Brightness temperature residual (TES-SHIS) comparison of TES with SHIS for TES 2A1(H_2O) filter. The red line indicates the microwindow regions TES uses for its retrievals.

cloud is assumed to be cirrus. This radiance closure study also provides valuable insight into the impact of clouds under these conditions. Forward model calculations with the CFH atmospheric state and retrieved cloud optical depths (Figure 11f) are compared with the calculations without clouds (Figure 11b). The results show that these cirrus type clouds have a significant impact on the water vapor resid-

uals near the surface and the retrieved surface temperature (retrieved surface temperature difference is 3 K). Since minimizing these residuals is the fundamental operation in the retrievals, it is important to reduce the retrieval uncertainty as much as possible under these conditions. Presently the TES operational retrieval of effective optical depths has large uncertainties for effective optical depths less than
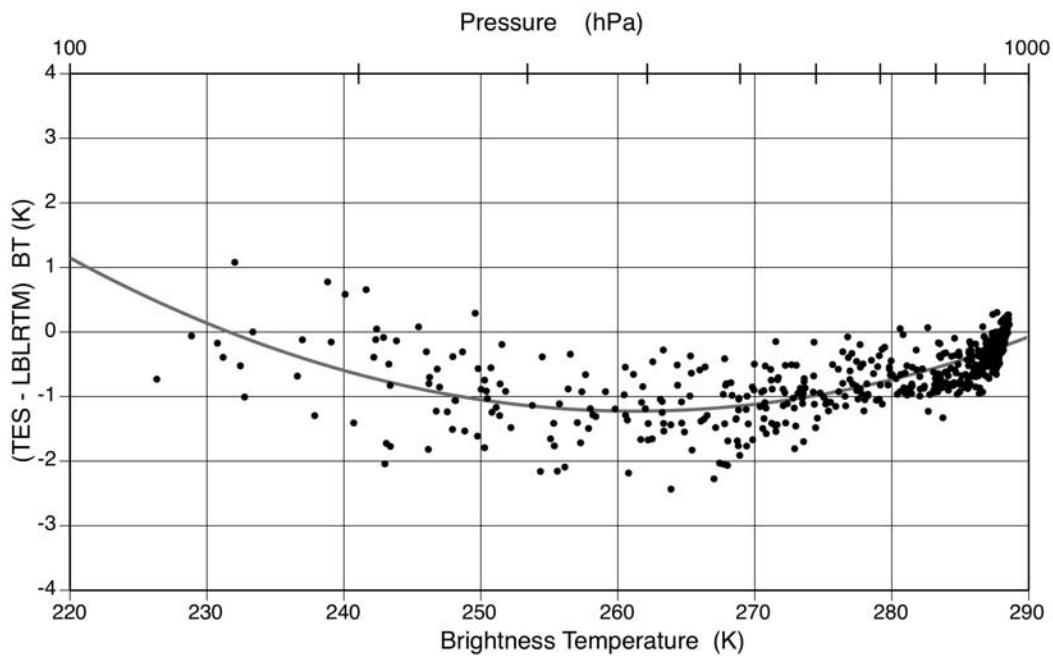

Figure 15. Scatterplot of TES – LBLRTM residuals versus the observed TES brightness temperatures for TES scan 20. The LBLRTM calculations were computed using the CFH profile. The pressure axis is only an approximate as it was generated assuming the observed brightness temperature closely represents the region in the CFH profile with the same temperature.

a few tenths and greater than two [*Kulawik et al.*, 2006b]. The radiance residuals from the TES reported uncertainties in the effective cloud optical depths are plotted in Figure 11g. Retrievals under these conditions are challenging and a number of refinements are being considered by the TES science team in order to reduce the uncertainty in the cloud retrievals. One possible approach would be to constrain the retrieval in such a way that the effective cloud optical depths represent the spectral signature of clouds, which will help distinguish retrieved clouds from other retrieved parameters (e.g., land surface emissivity). Another suggestion is to utilize more explicitly the TES interpixel variability in the retrieval process so that cloud-free cases can be more accurately identified, thus removing the impact of cloud uncertainty for these cases.

[37] Note that the forward model systematic errors are not likely the source of the radiance differences between the sonde and retrieval residual plots (i.e., Figures 11f and 11g) as the same forward model is used in all the calculations, therefore, they all contain the same systematic forward model error which will be mitigated by performing the differences of the residual plots.

[38] The same radiance closure analysis was performed for the two scans adjacent to scan 20. The results for scan 19 and scan 21 are shown in Figure 12 and Figure 13, respectively. A good coincidence is defined in terms of the magnitude of the brightness temperature residuals between the observations and the forward model calculations using the sonde. Comparing the magnitude of TES−sonde water vapor brightness temperature residuals in Figures 11–13 with their corresponding water vapor profiles results in Figures 8–10 show that the larger the brightness temperature residuals, the worse the spatial coincidence, and the greater the profile differences. For example, scan 20 has the smallest residuals ($\sim$1.5 K) and the best comparison profile comparison of in the middle troposphere with a peak difference of 40%, whereas scan 21 has the largest residual ($\sim$4 K) and has a peak difference of $\sim$100% at 400 mb. This shows that even for coincidences that are within 12 km and 1 h there can be large differences in water vapor observations, and that the sampling differences between the sondes and the instantaneous TES profiles account for most of the profile comparison differences.

5. Conclusions

[39] We first presented global comparisons of TES water vapor retrievals with nighttime NCEP Vaisala RS90 and RS92 radiosondes. The TES/radiosonde comparisons show a mean differences of <5% and a standard deviation of $\sim$20% in the lower troposphere (below $\sim$600 hPa) with the radiosonde being drier. This sonde dry bias compared with the TES observations increases to a maximum of $\sim$15% in the upper troposphere between $\sim$300−200 hPa. The standard deviation in this region reaches $\sim$40%. These global comparison results are comparable with the AIRS/radiosonde reported unweighted mean of 25% and RMS of $\sim$55%. Global comparisons with in situ water vapor measurements from radiosondes do help identify issues with satellite retrievals, but often the inherent sampling errors and radiosonde measurement accuracy limit the degree to which the sonde profiles alone can be used to validate TES

water vapor retrievals. We demonstrated that even under relatively benign conditions where there is a "very good" coincidence between TES and the sonde (e.g., 12 km and 1 h) there can be large differences mainly due to the fact the sonde is not sampling the same air mass as TES. Radiance closure studies and a suite of water vapor observations were used to help characterize the water vapor variability along the TES transect and help better understand the TES-sonde profile differences. TES shows a moist bias with respect to the sonde. However, results from the closure studies indicate that the estimated systematic errors from the forward model, TES measurements, CFH observations, and the retrieved temperature profile and clouds are likely not large enough to account for larger TES/sonde comparison differences. Therefore, either there are additional systematic errors that are not being accounted for in the estimates (e.g., cloud uncertainties, uncertainties in the sonde observations are larger than documented, etc.), or the differences are due to sampling errors. Forward model systematic errors (e.g., spectroscopic errors in the strong absorbing water vapor lines are larger than reported) are not likely the source of the radiance differences between the TES retrievals and the sondes as the same forward model is used to compute radiances from both the retrieved and sonde profiles; therefore, any systematic errors in the forward model will be mitigated by performing the differences of the differences between observed − forward model radiances from both profiles. The detailed comparison showed that the retrieval of cloud optical depths under these conditions must be done accurately as high clouds with optical depths of $\sim$10% can have a significant impact on the radiances used to retrieve the water vapor profile.

[40] In order to rigorously validate the TES water vapor retrievals, further detailed comparison studies are needed in which accurate coincident profile observations are identified from radiance closure studies and accompanied by a suite of other water vapor measurements that capture the water vapor variability and the clouds. The next step in the TES water vapor "validation" will be to perform water vapor comparisons with the purely vertical, remotely sensed profiles from the ground-based Raman lidar during WAVES_2006 and the proposed airborne Raman lidar measurements for WAVES_2007 [*Whiteman et al.*, 2006]. In addition, any coincident and colocated retrievals from interferometer instruments will be used for validations.

References

Beer, R. (2006), TES on the Aura mission: Scientific objectives, measurements and analysis overview, IEEE Trans, *Geosci. Remote Sens.*, *44*(5), 1102−1105, doi:10.1109/TGRS.2005.863716.

Beer, R., T. A. Glavich, and D. M. Rider (2001), Tropospheric emission spectrometer for the Earth Observing System's Aura satellite, *Appl. Opt.*, *40*, 2356–2367, doi:10.1364/AO.40.002356.

Bloom, S., et al. (2005), Documentation and validation of the Goddard Earth Observing System (GEOS) data assimilation system—Version 4, *Tech. Rep. Global Model. Data Assimilation 104606*, NASA, [location]. (Available at http://gmao.gsfc.nasa.gov/pubs)

Bowman, K. W., et al. (2006), Tropospheric emission spectrometer: Retrieval method and error analysis, *IEEE Trans. Geosci. Remote Sens.*, *44*(5), 1297–1307, doi:10.1109/TGRS.2006.871234.

Cady-Pereira, K. E., M. W. Shephard, D. D. Turner, E. J. Mlawer, S. A. Clough, and T. J. Wagner (2008), Improved total column precipitable water vapor from Vaisala RS90 and RS92 radiosonde humidity sensors, *J. Atmos. Oceanic Technol.*, doi:10.1175/2007JTECHA1027.1, in press.

Clough, S. A., M. J. Iacono, and J.-L. Moncet (1992), Line-by-line calculation of atmospheric fluxes and cooling rates: Application to water vapor, *J. Geophys. Res.*, *97*, 15,761–15,785.

Clough, S. A., M. W. Shephard, E. J. Mlawer, J. S. Delamere, M. J. Iacono, K. Cady-Pereira, S. Boukabara, and P. D. Brown (2005), Atmospheric radiative transfer modeling: A summary of the AER codes, *J. Quant. Spectrosc. Radiat. Transfer*, *91*, 233–244, doi:10.1016/j.jqsrt.2004.05.058.

Clough, S., et al. (2006), Forward model and Jacobians for Tropospheric Emission Spectrometer retrievals, *IEEE Trans. Geosci. Remote Sens.*, *44*(5), 1308–1323, doi:10.1109/TGRS.2005.860986.

Divakarla, M. G., C. D. Barnet, M. D. Goldberg, L. M. McMillin, E. Maddy, W. Wolf, and L. Zhou (2006), Validation of AIRS temperature and water vapor retrievals with matched radiosonde measurements and forecasts, *J. Geophys. Res.*, *111*, D09S15, doi:10.1029/2005JD006116.

Eldering, A., S. S. Kulawik, J. Worden, K. Bowman, G. Osterman, S. A. Clough, and M. Shephard (2008), Implementation of cloud retrievals for TES atmospheric retrievals: 2. Characterization of cloud top pressure and effective optical depth retrievals, *J. Geophys. Res.*, doi:10.1029/2007JD008858, in press.

Gordon, I. E., L. S. Rothman, R. R. Gamache, D. Jacquemart, C. Boone, P. F. Bernath, M. W. Shephard, J. S. Delamere, and S. A. Clough (2008), Current updates of water vapor linelist in HITRAN2004: A new "Diet" for air-broadened half-widths, *J. Quant. Spectrosc. Radiat. Transfer*, *108*, 389–402, doi:10.1016/j.jqsrt.2007.06.009.

Kulawik, S. S., G. Osterman, D. B. A. Jones, and K. W. Bowman (2006a), Calculation of altitude-dependent Tikhonov constraints for TES nadir retrievals, *IEEE Trans. Geosci. Remote Sens.*, *44*(5), 1334–1342, doi:10.1109/TGRS.2006.871206.

Kulawik, S. S., J. Worden, A. Eldering, K. Bowman, M. Gunson, G. B. Osterman, L. Zhang, S. A. Clough, M. W. Shephard, and R. Beer (2006b), Implementation of cloud retrievals for Tropospheric Emission Spectrometer (TES) atmospheric retrievals: part 1. Description and characterization of errors on trace gas retrievals, *J. Geophys. Res.*, *111*, D24204, doi:10.1029/2005JD006733.

Miloshevich, L. M., A. Paukkunen, H. Vömel, and S. J. Oltmans (2004), Development and validation of a time-lag correction for Vaisala radiosonde humidity measurements, *J. Atmos. Oceanic Technol.*, *21*, 1305–1327, doi:10.1175/1520-0426(2004)021<1305:DAVOAT>2.0.CO;2.

Miloshevich, L. M., H. Vömel, D. N. Whiteman, B. M. Lesht, F. J. Schmidlin, and F. Russo (2006), Absolute accuracy of water vapor measurements from six operational radiosonde types launched during AWEX-G and implications for AIRS validation, *J. Geophys. Res.*, *111*, D09S10, doi:10.1029/2005JD006083.

Osterman, G. (Ed.) (2006), *TES Level 2 Data User's Guide*, Jet Propul. Lab., Pasadena, Calif.

Raval, A., and V. Ramanathan (1989), Observational determination of the greenhouse effect, *Nature*, *342*, 758–761, doi:10.1038/342758a0.

Rodgers, C. D. (2000), *Inverse Methods for Atmospheric Sounding: Theory and Practice*, World Sci., Hackensack, N. J.

Rodgers, C. D., and B. J. Connor (2003), Intercomparison of remote sounding instruments, *J. Geophys. Res.*, *108*(D3), 4116, doi:10.1029/2002JD002299.

Rothman, L. S., et al. (2003), The HITRAN molecular spectroscopic database: Edition of 2000 including updates through 2001, *J. Quant. Spectrosc. Radiat. Transfer*, *82*, 5–44, doi:10.1016/S0022-4073(03)00146-8.

Schoeberl, M. R., et al. (2006), Overview of the EOS Aura mission, *IEEE Trans. Geosci. Remote Sens.*, *44*(5), 1066–1074, doi:10.1109/TGRS.2005.861950.

Shephard, M. W., et al. (2008), Tropospheric Emission Spectrometer nadir spectral radiance comparisons, *J. Geophys. Res.*, *113*, D15S05, doi:10.1029/2007JD008856.

Smith, W. L. (1991), Atmospheric soundings from satellites—False expectations or the key to improved weather prediction, *Q. J. R. Meteorol. Soc.*, *117*, 267–297.

Strow, L. L., S. E. Hannon, S. De-Souza Machado, H. E. Motteler, and D. C. Tobin (2006), Validation of the Atmospheric Infrared Sounder radiative transfer algorithm, *J. Geophys. Res.*, *111*, D09S06, doi:10.1029/2005JD006146.

Susskind, J., C. D. Barnet, and J. M. Blaisdell (2003), Retrieval of atmospheric and surface parameters from AIRS/AMSU/HSB data in the presence of clouds, *IEEE Trans. Geosci. Remote Sens.*, *41*, 390–409, doi:10.1109/TGRS.2002.808236.

Tobin, C. D., H. E. Revercomb, R. O. Knuteson, B. M. Lesht, L. L. Strow, S. E. Hannon, W. F. Feltz, L. A. Moy, E. J. Fetzer, and T. S. Cress (2006), Atmospheric Radiation Measurement site atmospheric state best estimates for Atmospheric Infrared Sounder temperature and water vapor retrieval validations, *J. Geophys. Res.*, *111*, D09S14, doi:10.1029/2005JD006103.

Turner, D. D., B. M. Lesht, S. A. Clough, J. C. Liljegren, H. E. Revercomb, and D. C. Tobin (2003), Dry bias and variability RS80-H radiosondes: The ARM experience, *J. Atmos. Oceanic Technol.*, *20*, 117–132, doi:10.1175/1520-0426(2003)020<0117:DBAVIV>2.0.CO;2.

Vömel, H., H. Selkirk, L. Miloshevich, J. Valverde, J. Valdés, E. Kyrö, R. Kivi, W. Stolz, G. Peng, and J. A. Diaz (2007a), Radiation dry bias of the Vaisala RS92 humidity sensor, *J. Atmos. Oceanic Technol.*, *24*(6), 953–963, doi:10.1175/JTECH2019.1.

Vömel, H., D. E. David, and K. Smith (2007b), Accuracy of tropospheric and stratospheric water vapor measurements by the cryogenic frost point hygrometer: Instrumental details and observations, *J. Geophys. Res.*, *112*, D08305, doi:10.1029/2006JD007224.

Whiteman, D. N., et al. (2006), Analysis of Raman lidar and radiosonde measurements from the AWEX-G field campaign and its relation to Aqua validation, *J. Geophys. Res.*, *111*, D09S09, doi:10.1029/2005JD006429.

Worden, J., S. S. Kulawik, M. W. Shephard, S. A. Clough, H. M. Worden, K. Bowman, and A. Goldman (2004), Predicted errors of Tropospheric Emission Spectrometer nadir retrievals from spectral window selection, *J. Geophys. Res.*, *109*, D09308, doi:10.1029/2004JD004522.

Worden, J., et al. (2007), Importance of rain evaporation and terrestrial sources in the tropical water cycle, *Nature*, *445*, doi:10.1038/nature05508.

———————————

M. Adam, Howard University, 2400 Sixth Street NW, Washington, DC 20059, USA.

R. Beer, K. W. Bowman, L. R. Brown, A. Eldering, B. M. Fisher, M. R. Gunson, R. L. Herman, S. S. Kulawik, M. Luo, G. B. Osterman, D. M. Rider, H. M. Worden, and J. R. Worden, Jet Propulsion Laboratory, 4800 Oak Grove Drive, Pasadena, CA 91109, USA.

K. E. Cady-Pereira, S. A. Clough, V. H. Payne, and M. W. Shephard, Atmospheric and Environmental Research Incorporated, 131 Hartwell Avenue, Lexington, MA 02421-3126, USA. (mshephar@aer.com)

J. P. Comer and D. N. Whiteman, Goddard Space Flight Center, NASA, 8800 Greenbelt Road, Greenbelt, MD 20740, USA.

R. Forno, University Mayor de San Andres, Monoblock Central Villazón Avenue N° 1995, La Paz 3165, Bolivia.

A. Goldman, University of Denver, 2199 S. University Boulevard, Denver, CO 80208, USA.

B. M. Lampel, Raytheon Technical Services Company, 299 N. Euclid Avenue, Suite 500, Pasadena, CA 91101-1544, USA.

L. M. Miloshevich, National Center for Atmospheric Research, 1850 Table Mesa Drive, Boulder, CO 80305, USA.

C. P. Rinsland, Langley Research Center, NASA, Hampton, VA 23681, USA.

C. D. Rodgers, Clarendon Laboratory, Oxford University, Parks Road, Oxford, OX1 3PU, UK.

H. Vömel National Oceanographic and Atmospheric Administration, 325 Broadway Street, Boulder, CO 80305, USA.